GEOLOGICA CARPATHICA, 53, 2, BRATISLAVA, APRIL 2002
79–85

REACTIONS BETWEEN Cr(VI) SOLUTIONS AND PYRITE: CHEMICAL AND SURFACE STUDIES

EMANUELE BENINCASA[1], MARIA FRANCA BRIGATTI[1*], GIANCARLO FRANCHINI[3], DANIELE MALFERRARI[1], LUCA MEDICI[2], LUCIANO POPPI[1] and MASSIMO TONELLI[4]

[1]Dipartimento di Scienze della Terra Dell'Università di Modena e Reggio Emilia, Modena, Italy
[2]IRA-CNR, Tito Scalo, Potenza, Italy
[3]Dipartimento di Chimica dell'Università di Modena e Reggio Emilia, Modena, Italy
[4]Centro Interdipartimentale Grandi Strumenti dell'Università di Modena e Reggio Emilia, Modena, Italy

(Manuscript received October 4, 2001; accepted in revised form December 13, 2001)

Abstract: Geochemical processes that result in the reduction of hexavalent chromium in natural waters with pyrite (FeS_2) have been studied at varying degrees of pH (from 1.2 to 12.6) and solution concentration (from 0.001 to 0.3 M of Cr(VI)) in order to demonstrate the differences in the proportions of elements between the aqueous and solid phases and to infer mechanisms that limit the Cr(VI) concentration in pore-waters in iron sulphide-rich environments. The experiments were carried out in the absence of oxygen and on pyrite grains previously treated to remove any oxide or sulphur layer at the mineral surface. The methods used to characterize reacting solutions and mineral surface comprised: chemical analyses (microprobe analyses and inductively coupled plasma analyses), scanning electron microscopy, atomic force microscopy and X-ray single crystal analysis. The results suggest that: 1) mineral dissolution increases with decreasing pH, whereas it is close to zero at pH > 7; at alkaline pH, the Cr(VI) reduction is very low and the decrease in total Cr probably indicates the formation of precipitated phases, like $FeCrO_4$, on the pyrite surface; 2) Cr(VI) reduction is significant at pH < 2.3. Cr(VI) to Cr(III) reduction involves the oxidation of Fe(II) and S_2^{2-} on the pyrite surfaces, following the reaction $2FeS_2 + 5Cr_2O_7^{2-} + 32H^+ \rightarrow 2Fe(OH)_3 + 4(SO_4)^{2-} + 10Cr^{3+} + 13H_2O$; 3) at acidic pH all the pyrite crystals show a variable Cr content on the surfaces.

Key words: chemical and surface analyses, redox reactions, pH, Cr(VI) solutions, pyrite crystals.

Introduction

Chromium can exist in several valence states, with trivalent Cr(III) and hexavalent Cr(VI) being the most common. These two oxidation states exhibit different chemical, biological, and environmental properties (Felter & Dourson 1997). Cr(III), which, at low concentrations, is considered to be a nutrient for humans (Felter & Dourson 1997), is thermodynamically stable in the environment over the pH range of most natural groundwaters, as a sorbed surface complex or in a solid phase (Anderson 1994; Gan et al. 1996). Cr(VI), on the other hand, a well known toxic contaminant (Xu et al. 1996), is stable as chromate (CrO_4^{2-}) or dichromate ($Cr_2O_7^{2-}$) anionic forms (Felter & Dourson 1997). Thus, reactions that reduce Cr(VI) to Cr(III) are important because they can promote the transition of a toxic, mobile element into a less toxic, immobile form.

The association of Fe(II)-bearing minerals (Fe-rich oxides, ferroan phlogopite and some clay minerals such as chlorite and corrensite) with Cr(VI) reduction has been documented by several authors. In particular, they have found that: i) at low pH, Fe(II) structurally linked to mineral structures is a stronger reducing agent than aqueous Fe(II) (White & Peterson 1996); ii) mixed-valence Cr(III)/(VI) effluents are reduced to Cr(III) when magnetite is present, whereas mixed valence Cr(III)/(VI) adsorbates or precipitated phases occur in soils without Fe(II) phases (White & Peterson 1996; Peterson et al. 1997); iii) the rate of reduction of Cr(VI) by Fe-rich phyllosilicates (chlorite, corrensite) depends on the Fe(II) mineral content and is more sensitive to pH than to temperature (Brigatti et al. 2000a). Furthermore, corrensite, which features both a high Fe(II)/Fe(III) ratio and a good exchange capacity, adsorbs the greatest amount of reduced Cr(III). X-ray absorption spectrometry studies (XAS) indicate changes at the Fe-K edge after the treatments (i.e., the decrease in Fe(II)/Fe(III) ratio) confirming that the mineral structures of both chlorite and corrensite are involved in the reactions (Brigatti et al. 2000b).

Fe-rich clays are commonly associated with Fe(II)-rich oxides and sulphides, which can participate to Cr(VI) reduction. Among them pyrite (FeS_2) is quite common. Owing to the high Fe(II) and S_2^{2-} contents, pyrite in soils can be a potential reducing agent for hexavalent chromium species in aqueous solutions, accounting for the overall equation:

$$2FeS_2 + 5Cr_2O_7^{2-} + 32H^+ \rightarrow 2Fe(OH)_3 + 4(SO_4)^{2-} + 10Cr^{3+} + 13H_2O \quad (1)$$

which promotes the reduction of Cr(VI). Several authors have studied reactions between metals in solution and sulphide minerals to assess: 1. their potential use in the treatment of metal-contaminated wastewaters deriving from the mineral extraction industry (Brown et al. 1979; Jean & Bancroft 1986; Zouboulis et al. 1992); 2. their role in the removal of metals from hydrothermal fluids to form ore deposits (Brookins 1976; Jean & Bancroft 1985); 3. their importance in governing the transport and reduction of transition metals in soils of contami-

* Maria Franca Brigatti, Department of Earth Sciences, University of Modena and Reggio Emilia Via S. Eufemia 19, 41100 Modena, Italy; Telephone number: +39-0592055805; Fax number: +39-0592055887; E-mail: brigatti@unimo.it

nated industrial waste landfill (Loyaux-Lawniczak et al. 2001).

However, few data describing the interaction between pyrite and Cr(VI) solution at different degrees of Cr(VI) concentration and pH are available. The present work increases the knowledge of the Cr(VI) to Cr(III) reduction by pyrite, in the absence of oxygen, at different Cr(VI) solution concentrations and in the pH range from 1.2 to 12.6, describing the modification of the pyrite surface after each treatment, the precipitated phases on pyrite surfaces, the mineral structure before and after treatments.

To achieve these aims we reacted pyrite crystals with solutions containing Cr(VI) in closed Teflon reactors and studied products (solution and pyrite) by a variety of methods, including chemical analyses, scanning electron microscopy, atomic force microscopy and X-ray single crystal analysis.

Materials and methods

Crystals of pyrite from Elba Island, part of the mineral collection of the Department of Earth Sciences, Modena and Reggio Emilia University, were selected for the experiments. Handpicked crystals were ground to a grain size of about 0.15 mm × 0.15 mm × 0.05 mm in a nitrogen atmosphere to avoid Fe(II) oxidation on the surface. The mineral sample was ultrasonically treated in ethanol for 30 min to free any small adhering particles. To remove any oxide layer that may have been formed on the mineral's surface in air, the mineral samples were treated in a 5% solution of HCl for several hours. Finally, the samples were put in carbon disulphide for several hours, dried and directly put in the Teflon reactors under a dry nitrogen atmosphere. This procedure was applied because several previous investigators had demonstrated that surface oxidation takes place as soon the surface comes into contact with oxygen or air (Raichur et al. 2000) and also to remove any elemental sulphur already present on the mineral surface (McGuire et al. 2001).

Untreated crystals were chemically and structurally characterized. The chemical composition of some natural crystals was determined using: 1) wavelength dispersive microprobe analyses (EPMA) performed with an ARL-SEMQ instrument (operating conditions: 20 kV accelerating voltage, 20 nA sample current and electron beam of about 3 μm spot size); 2) inductively coupled plasma Atomic-Emission Spectrometry (ICP-AES, Varian Liberty 200). ICP analysis was performed after a microwave digestion of 200 mg of sample with a HNO_3/HF mixture in closed Teflon crucibles. Structural determination was obtained on a crystal (0.10 × 0.15 × 0.04 mm) mounted on a Siemens P4P (Siemens 1993) rotating-anode single crystal diffractometer (graphite-monochromatized MoKα radiation, operating at 52 kV and 140 mA). Crystal structure refinement was performed using the SHELX-97 program (Sheldrick 1997) on selected ($I/\sigma > 3$) reflections.

To summarize, untreated pyrite features: 1) an Fe/S ratio of 0.87 in weight (0.50 in moles), which is very close to the stoichiometric value; 2) space group *Pa*3; 3) unit cell parameters $a = b = c = 5.4170(3)\times10^{-1}$ nm; 4) atomic positions and the refined bond distances (Fe-S = $2.2634(3)\times10^{-1}$ nm; S-S = $2.1623(8)\times10^{-1}$ nm) very close to those found by Fuji et al. (1986). We obtained the agreement factor at the end of three cycles of anisotropic refinement on 245 reflections obtained by averaging the collected 920 reflections for the half sphere (i.e. considering *P*1 symmetry, sometimes indicated for pyrite, Bayliss 1977) was $R = 0.026$.

The Cr(VI) treating solutions were prepared using CrO_3 and $K_2Cr_2O_7$. The pH was adjusted by the addition of H_2SO_4 and NaOH solutions. Analytical-grade reagents were added in deionized water and then the solutions were filtered through a 0.2-μm membrane filter prior to use. These solutions were mixed to obtain the Cr(VI) concentrations and pH values reported in Table 1. The amount of mineral to be used in each experiment, together with 100 ml of each solution, was 3.6 g. All suspensions were further purged with nitrogen for ~30 min and then the reactors were closed, protected from light, and shaken continuously at room temperature for 42 days. Details for each experiment are reported in Table 1. The experimental work mainly concerns the behaviour of the acid systems in response to slight variations in both pH and Cr(VI) concentrations. According to previous reports (Brigatti et al. 2000a,b), Cr(VI) to Cr(III) reduction in the presence of Fe(II) in solution is enhanced at pH < 3.

At the end of the reaction time (t = 42 days) the solid and the supernatant solution were immediately separated by centrifugation and analyzed for total Cr and Fe, and for Cr(VI). For each supernatant, total Cr and Fe were determined by ICP-AES. To evaluate Cr(VI)–Cr(III) reduction, the Cr(VI) content of the solution was determined by the lead nitrate method

Table 1: Number of the experiments, Cr(VI) solution concentration (M) used in each experiment, pH values of starting solution ($pH_{t=0}$), Cr(VI) (ppm) content in the starting solution ($Cr(VI)_{t=0}$), total Cr (ppm) ($Cr_{total\ (t=42\ days)}$), Cr(III)(ppm) ($Cr(III)_{(t=42\ days)}$), total Fe (ppm) ($Fe_{total\ (t=42\ days)}$) and pH values determined on the final solution (after 42 days of each treatment).

Experiment number	Cr(VI) M $_{t=0}$	$pH_{t=0}$	$Cr(VI)_{t=0}$	$Cr_{total\ (t=42\ days)}$	$Cr(III)_{t=42\ days}$	$Fe_{total\ (t=42\ days)}$	$pH_{t=42\ days}$
1	0.01	2.12	520	435.6	21.3	86.2	2.18
2	0.1	1.36	5200	4499.0	152.7	128.6	1.57
3	0.03	2.05	1560	1320.0	38.5	98.5	2.18
4	0.3	1.23	15600	14100.8	556	166.4	1.59
5	0.02	2.26	1040	839.3	28.3	72.3	2.40
6	0.2	1.29	10400	9168.6	453.8	147.1	1.57
7	0.001	7.16	52	43.9	0.6	0	7.13
8	0.01	7.47	520	420.5	1.8	0	7.44
9	0.01	10.13	520	399.5	2.2	0	9.90
10	0.001	12.56	52	26.7	0.1	0.31	12.12

(APHA 1985). The SO_4^{2-} amount in solution was analyzed by ion chromatography, as described by Violante et al. (1991). Calculations for Cr(VI) speciation at 0.1 M solution concentration were carried out using the MINTEQA2 program (Allison et al. 1991).

The pyrite crystals were studied before and after the experiments using a Scanning Electron Microscopy (SEM, Philips XL 40/604) device for their morphological features. The chemical composition of precipitates and treated-pyrite surfaces was obtained by an energy dispersive X-ray spectrometer (EDS, EDAX equipped with SEM). Mineral precipitates were identified by X-ray powder diffraction, using a Debye-Sherrer camera and CuKα radiation. Owing to their small size, precipitated phases were gently removed from several pyrite crystals from the same experiment using an optical microscope. In some cases, the variety of precipitates prevented phase identification.

Single crystal X-ray data collection and structure refinements were carried out on a treated pyrite crystal obtained from experiment 4 (0.3 M Cr(VI) solution concentration, pH = 1.23) to test structural variation after the experiments, following the same analytical methods adopted for untreated crystals. Atomic scale images of the crystal surface's microtopography were made on a Park Autoprobe CP Atomic Force Microscopy (AFM) in contact-mode using standard silicon nitride tips. Pyrite crystals were mounted on sample stubs with colloidal carbon suspended in alcohol and analyzed at room temperature. All AFM images were recorded in height mode, so that the quantitative measurement of the surface relief was possible. In the configuration used, AFM has angström-scale both for vertical and horizontal resolution. All images were collected at a variety of scan speeds and angles to reduce the possibility of image artefacts being created.

Results and discussion

The MINTEQA2 simulation results are shown in Fig. 1. At lower pH (0 < pH < 6) $Cr_2O_7^{2-}$, which is involved in the redox reaction (1), prevails in the solution. As the solution's pH increases, MINTEQA2 predicts that $Cr_2O_7^{2-}$ is substituted by CrO_4^{2-}, species that promotes the precipitation of mixed Cr(VI) and Fe(II) phases. The most likely forms are $FeCrO_4$, FeO

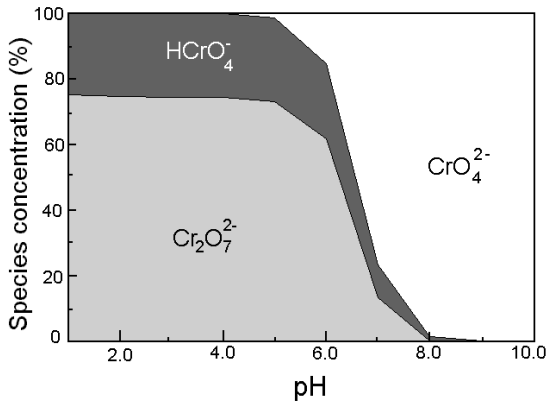

Fig. 1. Relevant Cr(VI) species vs. pH determined using the MINTEQA2 program (concentration of the Cr(VI) solution: 0.1 M).

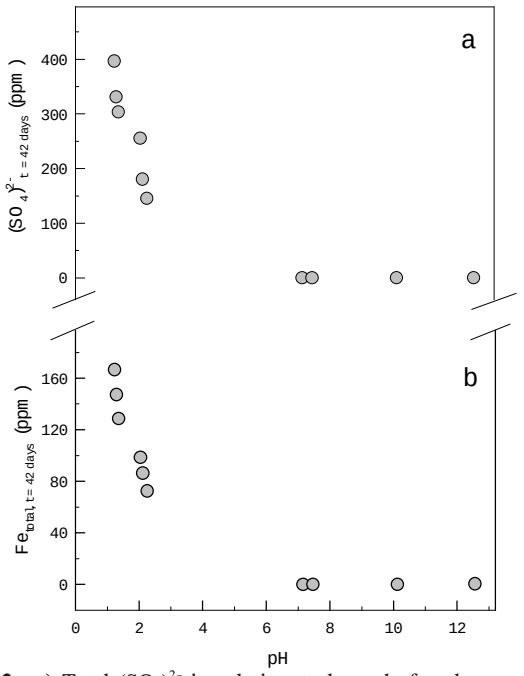

Fig. 2. a) Total $(SO_4)^{2-}$ in solution at the end of each experiment (t = 42 days) vs. the pH values of the starting solution; **b)** total Fe in solution at the end of each experiment (t = 42 days) vs. the pH values of the starting solution.

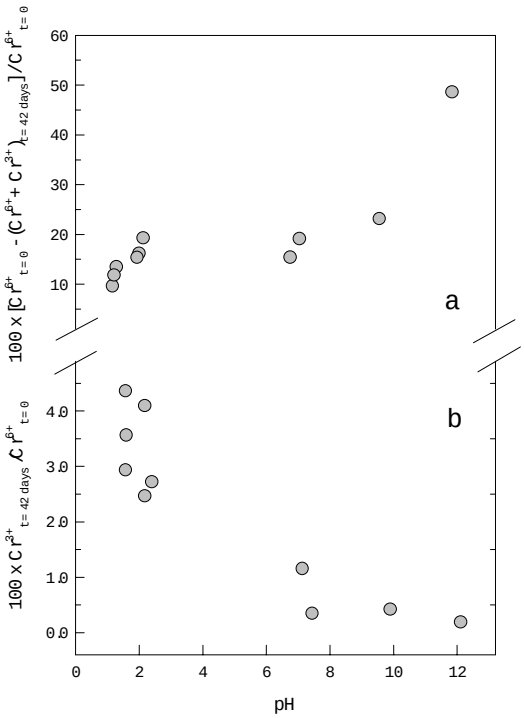

Fig. 3. a) Difference (%) between the Cr amount present in starting solution (t = 0) and the Cr amount at the end of the experiments (t = 42 days) vs. starting pH values; **b)** percentage of Cr(VI) to Cr(III) reduction at t = 42 days vs. starting pH values.

(wustite), $Fe^{2+}Fe_2^{3+}O_4$ (magnetite). Precipitated sulphur can occur over the whole pH range.

Analyses of starting and final solution composition indicated moderate changes for experiments 7 and 8, carried out in

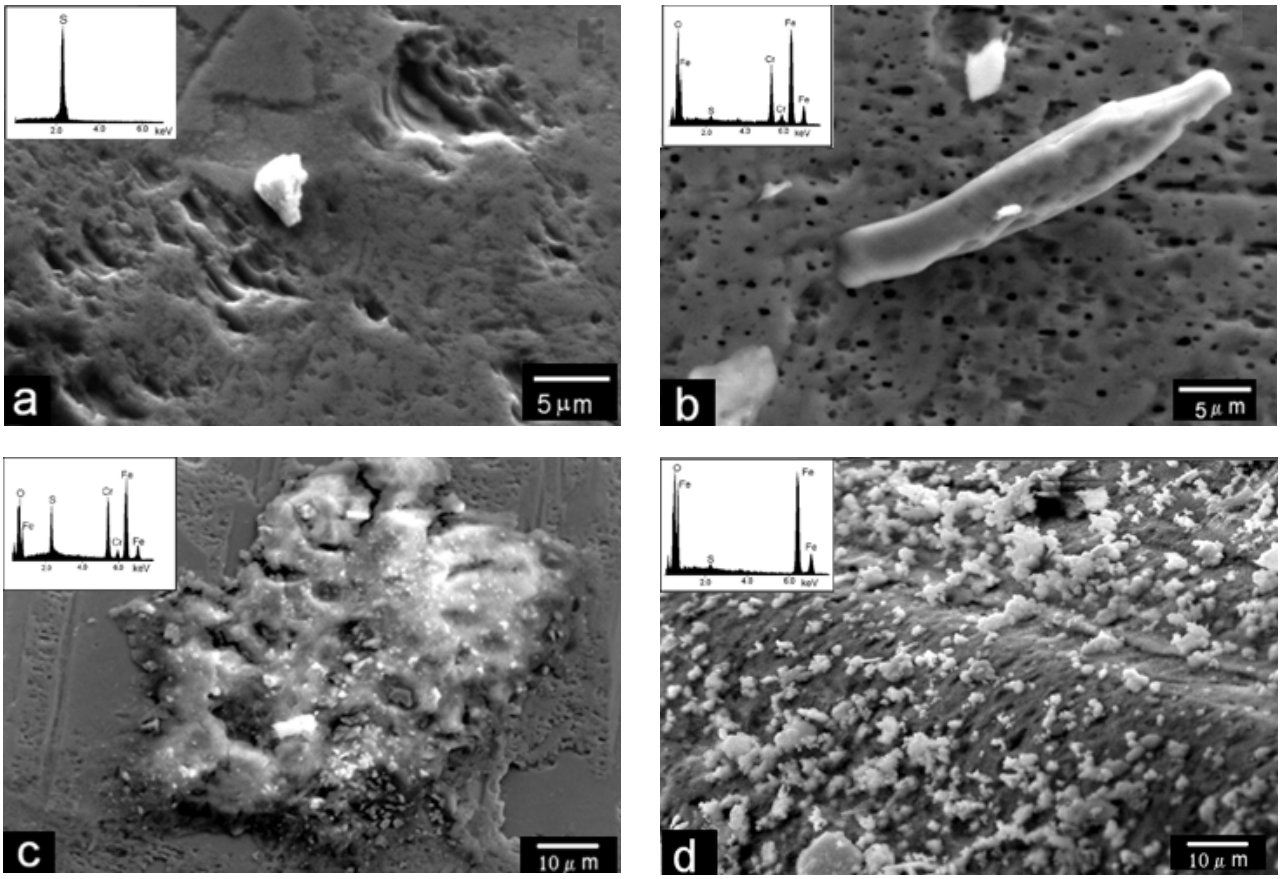

Fig. 4. SEM images and semiquantitative EDS-EDAX spectra for the pyrite crystals at the end of the experiments. **a)** Experiment 1; the spectrum refers to the grain at the center of the image. **b)** Experiment 6; the spectrum refers to elongated crystal. **c)** Experiment 8; the spectrum refers to the microcrystalline precipitate on the pyrite surface. **d)** Experiment 10; the spectrum refers to white aggregates.

nearly neutral environments, whereas significant changes were detected for experiments in acid environments. In particular: 1) acid systems show a small increase in pH value, whereas basic systems behave in an opposite manner (Table 1); 2) mineral dissolution increases with decreasing pH whereas it is close to zero in neutral and basic environments (Figs. 2a and 2b); 3) the decrease in final total Cr, mostly in neutral and basic environments, probably indicates the formation of precipitated phases on the pyrite surface (Fig. 3a); 4) the Cr(VI) reduction is very low in neutral and basic environments, whereas it is significant at pH < 2.3 (Fig. 3b); 5) iron and sulphur on pyrite surfaces may be chemically oxidized during Cr(VI) to Cr(III) reduction following the reaction (1).

However, to elucidate the mechanisms involved in pyrite–chromium-bearing aqueous solution systems, the mineral-water interface and the pathways of Fe and S oxidation must be considered in detail. The pyrite surface shows metal hydroxyl groups and thiol groups which protonate and deprotonate depending on pH changes (Park & Huang 1987; Dzombak & Morel 1990; Herbert et al. 2000):

$$Fe^{2+}\,S + H_2O \rightarrow Fe^{2+}\,S\,H_2O \rightarrow Fe^{2+}\,OHSH \qquad (2).$$

Thus, the pH of the solution not only drives the main redox processes, but also affects the features at the mineral-water interface.

In aqueous acid conditions Cr(VI) reduction can be explained by the following chemical processes related both to iron and sulphur oxidation:

$$6\,Fe^{2+} + Cr_2O_7^{2-} + 14\,H^+ \rightarrow 6\,Fe^{3+} + 2\,Cr^{3+} + 7\,H_2O \qquad (3)$$

and

$$3\,H_2S + Cr_2O_7^{2-} + H_2O \rightarrow 3\,S^0 + 2\,Cr^{3+} + OH^- \qquad (4).$$

S^0 can further contribute to Cr(VI) reduction following the reaction:

$$S^0 + Cr_2O_7^{2-} + 5\,H_2O \rightarrow (SO_4)^{2-} + 2\,Cr^{3+} + 6\,(OH)^- \qquad (5).$$

Fe(II) oxidation on pyrite surfaces in acid aqueous media depends on the reaction:

$$FeS_2 + 3.75\,O_2 + 2.5\,H_2O \rightarrow 2\,(SO_4)^{2-} + FeOOH + 4\,H^+ \qquad (6)$$

which produces ferric iron. Although, at low pH values, Fe(III) is considered a much more efficient oxidant for pyrite than oxygen (McKibben & Barnes 1986), the oxidative efficiency of the Cr(VI)/Cr(III) couple is higher than that of the Fe(III)/Fe(II) couple. Thus, we can assume that Cr(VI) to Cr(III) reduction proceeds and we can also justify the presence

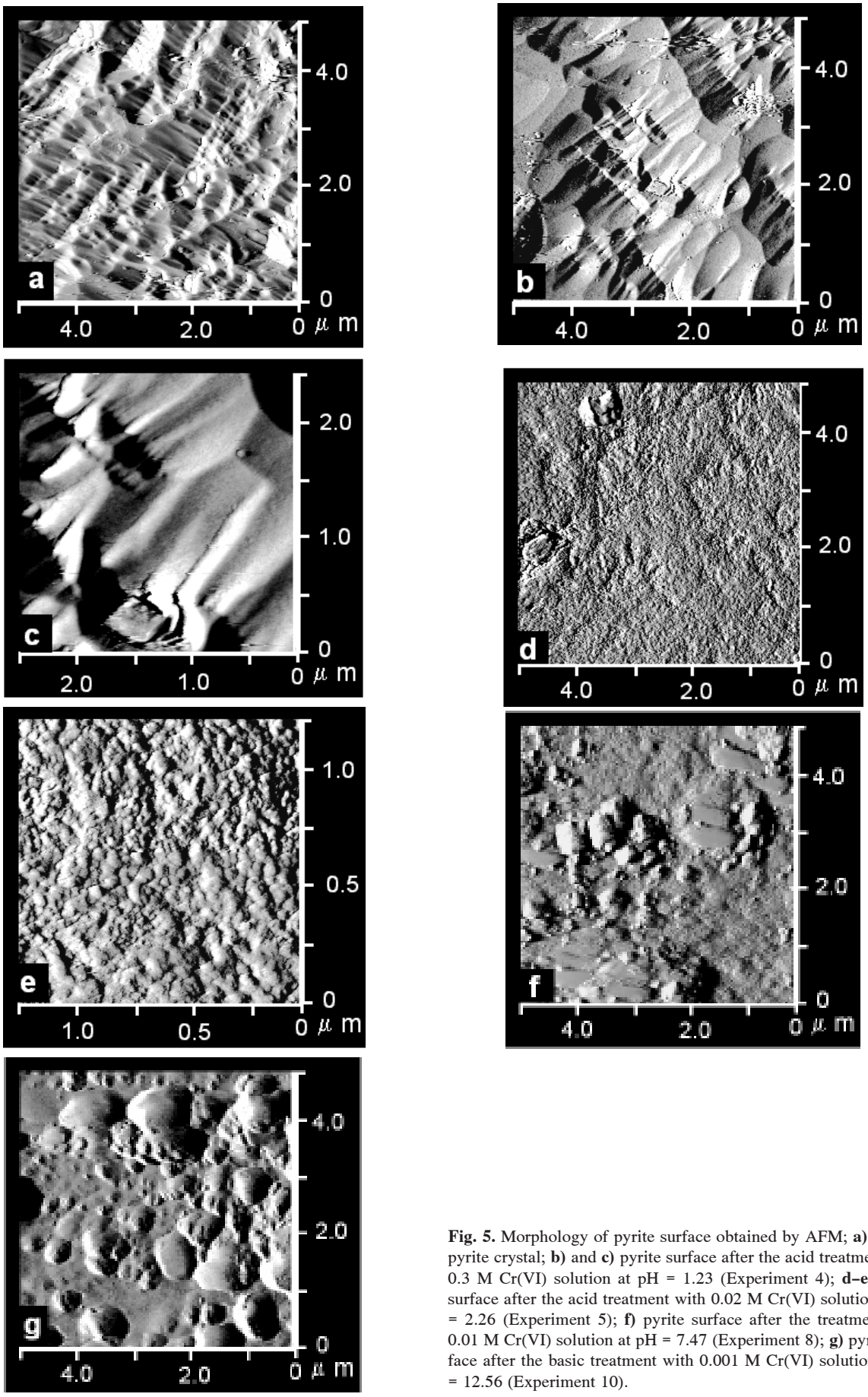

Fig. 5. Morphology of pyrite surface obtained by AFM; **a)** natural pyrite crystal; **b)** and **c)** pyrite surface after the acid treatment with 0.3 M Cr(VI) solution at pH = 1.23 (Experiment 4); **d–e)** pyrite surface after the acid treatment with 0.02 M Cr(VI) solution at pH = 2.26 (Experiment 5); **f)** pyrite surface after the treatment with 0.01 M Cr(VI) solution at pH = 7.47 (Experiment 8); **g)** pyrite surface after the basic treatment with 0.001 M Cr(VI) solution at pH = 12.56 (Experiment 10).

of a considerable amount of Fe(III) in solution. However, Fe(III) can reduce Fe(II) availability and it can therefore compete with Cr(VI) to promote Cr(VI)–Cr(III) reduction. At more basic pH, Cr(VI)–Cr(III) reduction is inhibited and the formation of Fe oxide coating on the grains may stop the pyrite oxidizing as well.

Reactions between the mineral surface and reduced Cr in solution (Cr(III)) may occur as: 1) precipitation reactions at the mineral-water interface to form pure Cr(III) or Fe(III)-phases or, most likely, solid–solution precipitates:

$$(1-x)\,Fe^{3+} + x\,Cr^{3+} + 3\,H_2O \rightarrow (Fe_{1-x}Cr_x)(OH)_3 + 3\,H^+ \qquad (7)$$

2) chemical adsorption involving surface functional groups and relatively stable inner sphere complexes in solution:

$$Fe^{3+}OH + Cr^{3+}(OH) \rightarrow Fe^{3+}OCr^{3+}(OH) + H^+ \qquad (8)$$

(where Fe^{3+} represents structural iron on mineral surfaces, whereas Cr^{3+} represents reduced chromium in solution); 3) electrostatic or physical adsorption involving charged hydrated ions in solution and oppositely charged mineral surfaces (Parks 1990; Davis & Kent 1990). All these mechanisms account for the decrease in total Cr content during the experiments; however, the complexity of the system prevents its interpretation by general and stoichiometric equations.

SEM/EDS and X-ray analysis of the reacted crystals revealed that the distribution of precipitates depends on the pH of the treatment solution. The precipitated phases and their chemical composition are shown in Figures 4a–4d. At acidic pH (pH < 2.3), small sulphur crystals were found on the mineral surface (Fig. 4a), while at neutral or slightly basic pH, Cr-Fe mixed phases were found. They can be well crystallized (Fig. 4b) or microcrystalline (Fig. 4c). X-ray powder patterns of microcrystalline deposits indicate a mixture of sulphur and $FeCrO_4$. At basic pH (pH = 12.56), precipitated FeO (wustite) and $Fe^{2+}Fe^{3+}_2O_4$ (magnetite) cover the mineral surface almost completely (Fig. 4d).

Figure 5 displays the AFM morphological images for unreacted and reacted pyrite surfaces. Here only seven selected images are presented from a larger series. Figure 5a shows the image of the unreacted pyrite surface which presents the typical streaking. At acid pH (pH = 1.23 and pH = 1.36; Figs. 5b–c), no precipitation was observed on the mineral surfaces. At slightly higher pH (Figs. 5d–e), it is evident that reaction occurs at the mineral-water interface surfaces. The size of the reaction products increases with increasing pH. The aggregate morphological features increase in height from ten nm to one hundred nm as the pH increases from 7.16 to 12.56. Figures 5f and 5g present the precipitate images at pH 10.13 and 12.56. The quite different morphological features of the precipitates account for the differences in their structure and chemistry.

The reaction with the Cr(VI)-bearing solution seems to affect only the mineral surface. The structural refinement on a treated crystal does not show any structural variation. These results point to the involvement of just the mineral surface in the reaction process. Thus, to regenerate the mineral's reaction capability it has to be returned to its untreated condition.

Concluding remarks

The concentration of Cr(VI) in water can be limited by mineral solubility controls or by adsorption on the mineral's surface. In all acid experiments, traces of adsorbed Cr were found on the pyrite surface, and both the reduction and dissolution of Cr(VI) were enhanced at acid pH. The abundance of iron oxides that cover the pyrite surface in basic environments limits Cr(VI) to Cr(III) reduction, as does basic pH itself. Unlike iron-rich phyllosilicates, such as corrensite, which, after reduction, sorb Cr(III) in structural sites (Brigatti et al. 2000a), the mechanisms involving pyrite can mostly be ascribed to mineral dissolution and the reaction of dissolved iron with Cr(VI). However, because Fe(II)-bearing sulphides can reduce Cr(VI), they may be useful in reducing Cr toxicity in contaminated environments.

Pyrite reveals a low efficiency in Cr(VI) to Cr(III) reduction respect to magnetite and ilmenite (White & Peterson 1996). At the end of the experiments, Cr(III) amount is always lower than 4.5 % of the total Cr starting amount (Table 1) and the Cr(VI) reduction is constrained in acidic environments.

Acknowledgments: The Italian MURST and CNR supported our research program.

References

Allison J.D., Brown D.S. & Novo-Gradac K.J. 1991: MINTEQA2/PRODEFA2, a geochemical assessment model for environmental systems: version 3.0 user's manual. *Environmental Research Laboratory, Office of Research and Development, U.S. Environmental Protection Agency*, Athens, Georgia 30613.

Anderson R.A. 1994: Nutritional and toxicological aspects of chromium intake: An overview. In: Mertz W., Abernathy C.O. & Olin S.S. (Eds.): Risk assessment of essential elements. *ILSI Press*, Washington D.C., 187–196.

APHA, AWWA, WPC 1985: Standard Methods for Examination of Water and Wastewaters, 17th edition. *American Public Health Association*, Washington D.C., 201–204.

Bayliss P. 1977: Crystal structure refinement of a weakly anisotropic pyrite. *Amer. Mineralogist* 62, 1168–1172.

Brigatti M.F., Franchini G., Lugli C., Medici L., Poppi L. & Turci E. 2000a: Interactions between aqueous chromium solutions and layer silicates. *Applied Geochemistry* 15, 1307–1316.

Brigatti M.F., Lugli C., Cibin G, Mottana A., Marcelli A., Wu Z., Giuli G. & Paris E. 2000b: Reduction and sorption of chromium by Fe(II)-bearing phyllosilicates: Chemical treatments and X-ray absorption spectroscopy studies. *Clays and Clay Miner.* 48, 272–281.

Brookins D.G. 1976: Position of uraninite and/or coffinite accumulation to the hematite-pyrite interface in sandstone-type deposits. *Econ. Geol.* 71, 944–948.

Brown J.R., Bancroft G.M. & Fyfe W.S. 1979: Mercury removal from water by iron sulphide minerals. An electron spectroscopy for chemical analyses (ESCA) study. *Environ. Sci. Technol.* 13, 1142–1144.

Davis J.A. & Kent D.B. 1990: Surface complexation modelling in aqueous geochemistry. In: Hochella M.F. & White A.F. (Eds.): Mineral-water interface geochemistry. *Rev. in Mineralogy* 23, 177–260, MSA.

Dzombak D.A. & Morel M.M. 1990: Surface complexation model-

ling. *John Wiley & Sons,* 1–393.

Felter S.P. & Dourson M.L. 1997: Hexavalent chromium-contaminated soils: option for risk assessment and risk management. *Regulatory Toxicology and Pharmacology* 25, 43–59.

Fujii T., Yoshida A., Tanaka K., Marmo F. & Noda Y. 1986: High pressure compressibilities of pyrite and cattierite. *Min. Journ. of Japan* 13, 202–211.

Gan H., Bailey G.W. & Yu S.Y. 1996: Morphology of lead(II) and chromium(III) reaction products on phyllosilicate surfaces as determined by Atomic Force Microscopy. *Clays and Clay Miner.* 44, 734–743.

Herbert R.B., Benner S.G. & Blowes D.W. 2000: Solid phase iron-sulfur geochemistry of a reactive barrier for treatment of mine drainage. *Appl. Geochem.* 15, 1331–1343.

Jean G.E. & Bancroft G.M. 1985: An XPS and SEM study of gold deposition at low temperatures on sulphide mineral surfaces: concentration of gold by adsorption/reduction. *Geochim. Cosmochim. Acta* 49, 979–987.

Jean G.E. & Bancroft G.M. 1986: Heavy metal adsorption by sulphide mineral surfaces. *Geochim. Cosmochim. Acta* 50, 1455–1463.

Loyaux-Lawniczak S., Lecomte P. & Ehrhardt J.-J. 2001: Hexavalent chromium in a polluted groundwater: Redox processes and immobilization in soils. *Environ. Sci. Technol.* 35, 1350–1357.

McGuire M.M., Jallad K.N., Ben-Amotz D. & Hamers. R.J. 2001: Chemical mapping of elemental sulfur on pyrite and arsenopyrite surfaces using near-infrared Raman imaging microscopy. *Appl. Surface Sci.* 178, 105–115.

McKibben M.A. & Barnes H.L. 1986: Oxidation of pyrite in low temperature acidic solutions: rate laws and surface textures. *Geochim. Cosmochim. Acta* 50, 1598–1520.

Park S.W. & Huang C.P. 1987: The surface acidity of hydrous CdS (s). *J. Colloid Interface Sci.* 117, 431–441.

Parks G.A. 1990: Surface energy and adsorption at mineral/water interfaces: an introduction. In: Hochella M.F. & White A.F. (Eds.): Mineral-water interface geochemistry. *Rev. in Mineralogy* 23, 133–176, MSA.

Peterson M.L., Brown G.E., Parks G.A. & Stein C.L. 1997: Differential redox and sorption of Cr(III/VI) on natural silicate and oxide minerals: EXAFS and XANES results. *Geochim. Cosmochim. Acta* 61, 3399–3412.

Raichur A.M., Wang X.H. & Parekh B.K. 2000: Quantifying pyrite surface oxidation kinetics by contact angle measurements. *Colloids and Surfaces A* 167, 245–251.

Sheldrick G. M. 1997: The SHELX-97 Manual. *Göttingen University*, Germany.

Siemens 1993: XSCANS: X-ray Single Crystal Analysis System. *Techn. Ref. Siemens Instr.*

Violante A., Colombo C. & Buondonno A. 1991: Competitive adsorption of phosphate and oxalate by aluminum oxides. *Soil Sci. Soc. Am. J.* 55, 65–70.

White A.F. & Peterson M.L. 1996: Reduction of aqueous transition metal species in the surfaces of Fe(II)-containing oxides. *Geochim. Cosmochim. Acta* 60, 3799–3814.

Xu J., Bubley G.J., Deteric B., Blankenship I.J. & Patierno S.R. 1996: Chromium(VI) treatment of normal human lung cells results in guanine-specific DNA polymerase arrest. DNA-DNA cross links and S phase blockade of cell cycle. *Carcinogenesis* 17, 1511–1517.

Zouboulis A.I., Kydros K.A. & Matis K.A. 1992: Adsorbing flotation of copper hydroxo precipitates by pyrite. *Separation Science Technology* 27, 2143–2155.